

# A Bio-Inspired Biped Water Running Robot Incorporating the Watt-I Planar Linkage Mechanism

Linsen Xu<sup>1</sup>, Tao Mei<sup>1</sup>, Xianming Wei<sup>2</sup>, Kai Cao<sup>3</sup>, Mingzhou Luo<sup>1</sup>

1. Hefei Institutes of Physical Science, Chinese Academy of Science, Hefei 230031, P. R. China

2. University of Science and Technology of China, Hefei 230026, P. R. China

3. Changzhou Institute of Advanced Manufacturing Technology, Changzhou 213164, P. R. China

---

## Abstract

In this paper, a biped water running robot is developed by mimicking the water-running pattern of basilisk lizards. The dynamic mechanism of the robot was studied based on Watt-I planar linkages, and the movement trajectory of the double bar Assur Group was deduced to simulate the water-running foot trajectories of the basilisk lizard. A Central Pattern Generator (CPG)-based fuzzy control method was proposed to control the robot for realizing balance control and gait adjustment. The effectiveness of the proposed control method was verified on the prototype of a water running robot (weight: 320 g). When the biped robot is running on water, the average force generated by the propulsion mechanism is 1.3 N, and the robot body tilt angle is 5°. The experiment results show that the propulsion mechanism is effective in realizing the basilisk lizards-like water running patterns, and the CPG-based fuzzy control method is effective in keeping the balance of the robot.

**Keywords:** bio-inspired robot, basilisk lizards-like robot, biped water running, CPG-based fuzzy control

Copyright © 2013, Jilin University. Published by Elsevier Limited and Science Press. All rights reserved.  
doi: 10.1016/S1672-6529(13)60236-X

---

## 1 Introduction

The requirement of the amphibious function of robots is brought out to implement the works such as military surveillance, water quality monitoring, wetland detection, and search in complex environments. The technologies of legged robots walking on hard land surface are mature relatively<sup>[1,2]</sup>, so it has been a hot research topic in robotics area to study the key technologies of legged robots walking on different kinds of material surface, such as water and soft sand, to expand their application range.

Boxerbam *et al.*<sup>[3,4]</sup> developed an amphibious robot, Whlegs IV, which used three simplified wheeled legs to imitate the functions of the cockroach legs. The robot can walk on land and swim in water. Hobson *et al.*<sup>[5]</sup> developed an amphibious robot, Madeleine, which has two parallel fins as the actuating devices. The robot can walk on seabed and beach, and swim in water.

However, the aforementioned amphibious robots can only move in water slowly, which can not satisfy the requirements of rescue and military surveillance on

water surface. Under such condition, several amphibious robots that can run on water have been developed. Song *et al.*<sup>[6]</sup> developed a robot with twelve legs, which can run on water by mimicking the water strider. The robot floats by using the surface tension of water and moves by driving the special paddle-type legs, which results in low payload (9.3 g) and low walking speed (3 cm·s<sup>-1</sup>). Floyd *et al.*<sup>[7]</sup> developed a quadruped robot, which realized the water running function by its four disk feet striking water<sup>[7]</sup>. The payload of this robot is about 50 g.

Basilisk lizards are capable of walking across the water surface at approximately a speed of 1.5 m·s<sup>-1</sup> using their hind legs with a stride frequency of 5 Hz to 10 Hz (per leg). Compared with ships, the basilisk lizards' movement can reduce the viscous drag of water surface, which can improve the propulsive efficiency.

In this paper, a novel biped robot inspired by basilisk lizards was developed to improve the payload and simplify the control method of the water running robot. Firstly, we emulated the water running function of basilisk lizards by a Watt-I six-bar linkage, and developed the propulsion mechanism. Secondly, a CPG-fuzzy

control method was adopted to design the robot's control system. Finally, we implemented the prototype of the robot and tested its water running ability. The experimental results confirmed the effectiveness of the proposed propulsion mechanism and control method.

Different with the quadruped water running robot developed by Stitti *et al.*<sup>[7,8]</sup>, the robot in this paper is biped. Compared with the quadruped robot foot moving with a constant angle, the angle of the biped robot foot varies to be parallel to the water surface when it is slapping the water surface. The biped method is more beneficial for robot energy saving and balance keeping when compared with the quadruped water running method, and the biped robot gait is more simple to control.

### 2 Dynamics of biped water running robot

The stride of a basilisk lizard in water running can be divided into three phases: slap, stroke, and recovery, as shown in Fig. 1<sup>[9]</sup>. The propulsion forces generated by the feet are different in each phase. Surface tension effects on the ability to run on water are much less than the propulsion forces, and which are neglected in this case. The trajectories of the knee, the ankle and the foot of one leg of the lizard can be considered in a plane approximately, as shown in Fig. 2<sup>[8]</sup>.

We implement the water running function of the biped robot by simulating the foot trajectory of basilisk lizard. The stride of the robot is also divided into three phases: slap, stroke and recovery. In the slap and stroke phases, the lizard pushes against the water beneath its foot by stroking downward the foot and creating an air cavity in water. The momentum transfers from the foot to the water during this slap, and stroke phase generates the lift force to stay afloat and the main propulsion force to thrust forward. The force for a foot entering the water is<sup>[8]</sup>

$$F_{str}(t) = C_D^*[0.5S\rho \cdot v^2 + S\rho \cdot gh(t)], \quad (1)$$

where  $C_D^* \approx 0.703$  is the constant drag coefficient,  $\rho$  is the density of water,  $g$  is the acceleration of gravity,  $S$  is the area over which drag is occurring, and  $h(t)$  is the time varying depth of the foot. As reported in Ref. [8], this equation holds true over a large range of velocities for both lizards and experimental equipment.

The water reaction force curve on the foot in a stride can be formulated with respect to the above equation, as shown in Fig. 3. The water reaction force on

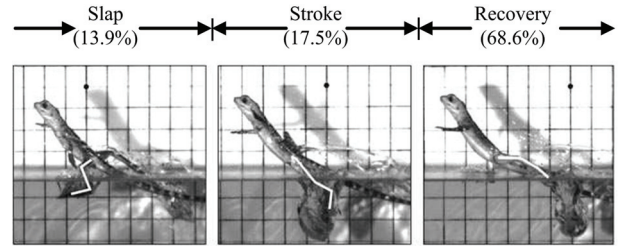


Fig. 1 Pictures of a basilisk lizard running on water<sup>[9]</sup>.

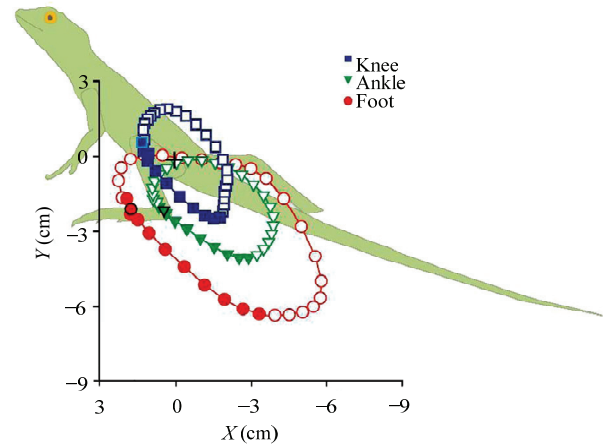


Fig. 2 Movement trajectories of a basilisk lizard running on water<sup>[8]</sup>.

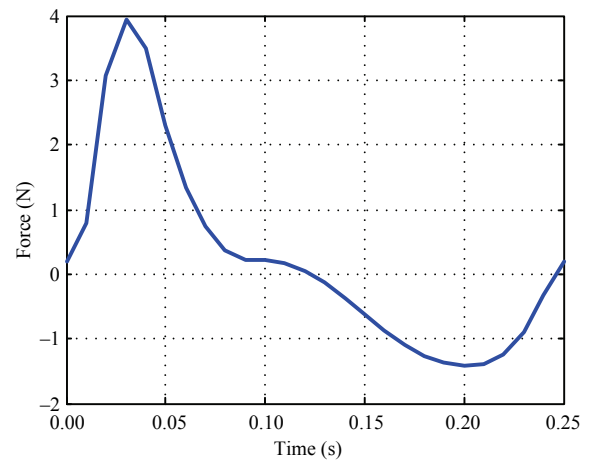


Fig. 3 Force curve during the robot running on water surface in simulation environment

the foot is positive during the slap and stroke phases, namely,  $t \in [0, 0.12]$ , so the force will lift and propel the robot during the slap and stroke phases. The force is negative during the recovery phase, namely,  $t \in [0.12, 0.25]$ , so the force will lower and resist the robot.

### 3 Propulsion mechanism design

The double bar Assur Group of Watt-I linkage moves with similar method of the foot of basilisk lizards,

which can produce not only translational but also rotary motion<sup>[10]</sup>. The motion method can make the robot foot parallel to water surface at the beginning of the slap phase, and make  $S$  be zero at the beginning of the recovery phase, so the lifting and propulsion will be bigger and the drag force will be smaller. Therefore, an improved Watt-I linkage is adopted to design the propulsion mechanism. Watt-I linkage is shown as Fig. 4, and the double bar Assur Group are the rod group which link the connecting linkage and output linkage of the grounded four-bar linkage.

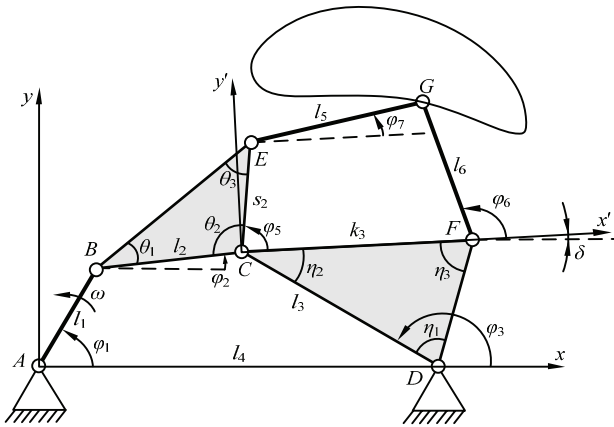


Fig. 4 Watt-I planar linkage.

### 3.1 Kinematic analysis of double bar Assur group of Watt-I linkage

The double bar Assur group will not constrain the four-bar linkage as long as the following conditions are satisfied

$$\begin{cases} \max\{EF\} \leq |EG| + |FG| \\ \left| |EG| - |FG| \right| \leq \min\{EF\} \end{cases} \quad (2)$$

In Fig. 4, the links of  $AB$ ,  $BC$ ,  $CD$  and  $AD$  constitute the grounded four-bar linkage, whose lengths are represented by  $l_1$ ,  $l_2$ ,  $l_3$  and  $l_4$ , respectively. Suppose that the angles between the links  $AB$ ,  $BC$ ,  $CD$  and the  $x$ -axis are  $\varphi_1$ ,  $\varphi_2$ ,  $\varphi_3$  respectively, and the interior angles of  $\triangle BCE$  and  $\triangle DCF$  are  $\theta_i$  and  $\varphi_i$  ( $i = 1, 2, 3$ ), respectively. The link  $AB$  is the driving rod with a constant angular velocity of  $\omega$ . So the angular displacements can be described as<sup>[11]</sup>

$$\begin{cases} \varphi_3 = 2 \tan^{-1} \frac{N + \sqrt{M^2 + N^2 - Q^2}}{M - Q} \\ \varphi_2 = \tan^{-1} \frac{N + l_3 \sin \varphi_3}{M + l_3 \cos \varphi_3} \end{cases}, \quad (3)$$

where  $M = l_4 - l_1 \cos \varphi_1$ ,  $N = -l_1 \sin \varphi_1$ ,  $Q = \frac{M^2 + N^2 + l_3^2 - l_2^2}{2l_3}$ ,

and  $\varphi_1 = \omega t$ .

The trajectory of the point  $C$  can be deduced from

$$\begin{pmatrix} x_C \\ y_C \end{pmatrix} = \begin{pmatrix} l_1 \cos \varphi_1 + l_2 \cos \varphi_2 \\ l_1 \sin \varphi_1 + l_2 \sin \varphi_2 \end{pmatrix}. \quad (4)$$

The mechanism of  $ABCD$  is a quadrilateral, and

$$\begin{aligned} \angle BCD &= 2\pi - \varphi_1 - (\varphi_2 + \pi - \varphi_1) - (\pi - \varphi_3) \\ &= \varphi_3 - \varphi_2. \end{aligned} \quad (5)$$

Let  $\angle ECF = \varphi_5$ , and  $\varphi_5$  can be deduced as

$$\varphi_5 = 2\pi - \theta_2 - \eta_2 - (\varphi_3 - \varphi_2). \quad (6)$$

A new coordinate system  $x'Cy'$  is built by setting the point  $C$  as the origin and  $CF$  as the  $x'$ -axis, the angle between the  $x'$ -axis and the  $x$ -axis is then formulated as

$$\delta = \pi - \eta_3 - (\pi - (\varphi_3 - \eta_1)) = \varphi_3 - \eta_3 - \eta_1. \quad (7)$$

The links of  $CE$ ,  $EG$ ,  $GF$  and  $CF$  constitute a four-bar linkage also, and the lengths are represented as  $s_2$ ,  $l_5$ ,  $l_6$  and  $k_3$  respectively. The link  $CE$  is used as the driving link. Suppose that the angles between the rods  $EG$ ,  $FG$  and the  $x'$ -axis are  $\varphi_7$  and  $\varphi_6$ , respectively, and the angular displacements can be known as

$$\begin{cases} \varphi_6 = 2 \tan^{-1} \frac{J + \sqrt{H^2 + J^2 - K^2}}{H - K} \\ \varphi_7 = \tan^{-1} \frac{J + l_6 \sin \varphi_6}{H + l_6 \cos \varphi_6} \end{cases}, \quad (8)$$

where  $H = k_3 - s_2 \cos \varphi_5$ ,  $J = -s_2 \sin \varphi_5$ ,  $K = \frac{H^2 + J^2 + l_6^2 - l_5^2}{2l_6}$ .

So the trajectory of the point  $G$  in the coordinate system  $x'Cy'$  can be deduced from

$$\begin{pmatrix} x'_G \\ y'_G \end{pmatrix} = \begin{pmatrix} s_2 \cos \varphi_5 + l_5 \cos \varphi_7 \\ s_2 \sin \varphi_5 + l_5 \sin \varphi_7 \end{pmatrix}. \quad (9)$$

The trajectory of point  $G$  in the coordinate system  $xAy$  can be got by the coordinate transformation

$$\begin{pmatrix} x_G \\ y_G \end{pmatrix} = \begin{pmatrix} x'_G \cos \delta - y'_G \sin \delta + x_C \\ y'_G \sin \delta + x'_G \cos \delta + y_C \end{pmatrix}. \quad (10)$$

The trajectory of point  $G$  is shown in Fig. 4.

### 3.2 Virtual design of propulsion mechanism

The trajectory of point  $G$  shown in Fig. 4 is similar with the foot trajectory shown in Fig. 2, so we can use the improved Watt-I mechanism as the propulsion mechanism of the biped robot.

The number  $F_b$  of the Degree-of-Freedom (DOF) of the mechanism is got as

$$F_b = 3n - 2P_L - P_H = 3 \times 5 - 2 \times 7 - 0 = 1, \quad (11)$$

where  $n$  is the number of moving links of the mechanism,  $P_L$  is the number of lower pairs of the mechanism, and  $P_H$  is the number of high pairs of the mechanism. Eq. (11) shows that the input number equals the degree number of the mechanism freedom, so the mechanism has a certain law of motion.

We use  $G$  as the center point of the robot's foot, and let it move under the  $x$ -axis to realize the stroke function of the propulsion mechanism. Simultaneously the triangle plates are replaced by the slender rods. So  $\theta_1 = \pi$  and  $\eta_1 = 0$ , and from the above equations we have  $\theta_2 = \theta_3 = \eta_2 = 0$ ,  $\eta_3 = \pi$  and

$$\begin{cases} \varphi_5 = 2\pi - \varphi_3 + \varphi_2 \\ \delta = \varphi_3 - \pi \end{cases} \quad (12)$$

Moreover, we rotate the link  $AD$  with an angle less than  $\pi/4$  around point  $A$  to ensure the foot be parallel to the water surface, which makes the lifting and propulsion force may be bigger. The final skeleton of the lifting and propulsion mechanism is shown as Fig. 5.

It can be known from Fig. 1 that the two feet slap the water surface alternatively during the lizard running on water. To mimic the water-running function of basilisk lizard, we use the same mechanisms for both side feet of the robot. The mechanisms are driven by one servo-motor, but the phase difference between them is  $\pi$ . The major structure of the biped robot is shown in Fig. 6<sup>[12]</sup>.

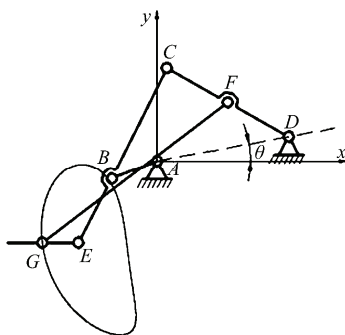


Fig. 5 Skeleton of the robot propulsion mechanism.

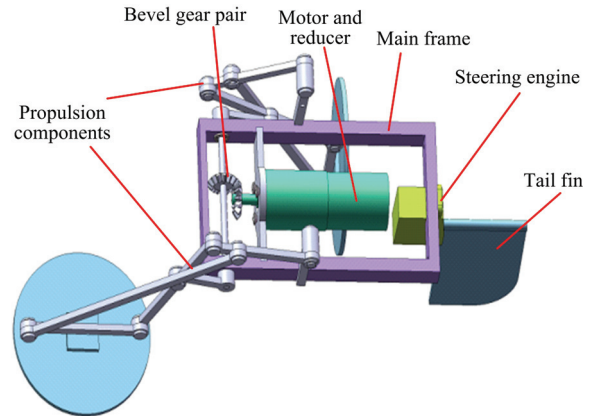


Fig. 6 Major structure of the biped water running robot.

Inspired by the balance systems such as an inverted pendulum, a balance apparatus is attached to the robot as Fig. 6. The apparatus is a tail fin powered by a steering engine, which uses the torque compensation to keep the body balance.

### 4 Robot motion control method

The Zero Moment Point (ZMP) criterion is adopted by most biped robots to keep balance<sup>[13,14]</sup>. However, when the biped robot is running on water, the air caves will come into being, and the disturbances of water blast and splash are more complex than typical land walking biped robot. We thus present a CPG-based effective gait adjustment method for the balance control of the biped water running robot.

Furthermore, since fuzzy control method has the characteristics of fuzziness, empirical and robustness, and normally the accurate mathematical model of the controlled object is not necessarily required, so fuzzy-based control method is especially suitable for complex system with nonlinearity, time-varying and large time delay.

In the following, we propose a CPG-based fuzzy control algorithm for the biped water running robot for realizing balance control and gait adjustment.

#### 4.1 Modeling of CPG-based fuzzy controller

The CPG-based fuzzy control is a control method inspired by the lower nerve center of living beings<sup>[15]</sup>. The CPG controller for the water running robot is built by two improved Hopf models

$$\begin{cases} m_i' = (\mu_i - \gamma_i^2)m_i + \omega n_i + \sum_{j=1, j \neq i}^n a_j m_j \\ n_i' = (\mu_i - \gamma_i^2)n_i - \omega m_i \end{cases} \quad (13)$$

where  $\gamma_i = \sqrt{m_i^2 + n_i^2}$  ( $i = 1, 2$ ),  $m_i$  are the output signals of the CPG controller,  $n_i$  are the intermediate variables of the CPG controller,  $\mu_i$  and  $\omega$  are the state variables of the CPG controller, and  $\Sigma a_j m_j$  are the connective signals of the other oscillators,

We set different values (Table 1) for the variables of Eq. (13), and the outputs of the CPG controller are shown as Fig. 7.

**Table 1** Corresponding output of the different variables

	$\mu_1$	$\mu_2$	$\omega$	$a_1$	$a_2$	Oscillogram
No.1	1	5	1.0	0.1	-0.1	Fig. 7a
No.2	1	1	0.2	0.1	-0.1	Fig. 7b
No.3	1	1	0.4	0.3	-0.3	Fig. 7c
No.4	1	1	0.4	-0.3	0.3	Fig. 7d

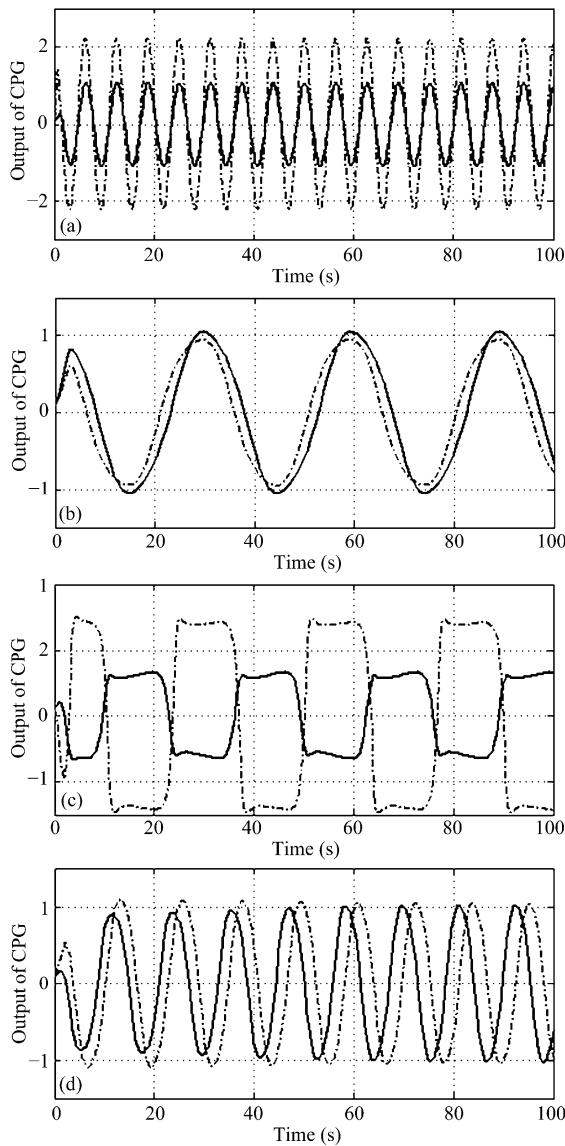


**Fig. 7** Outputs of the Hopf controller with different variable values.

It can be known from Fig. 7 that the output signals with different phase relations such as  $0, \pi, \pi/2$  and so on can be got by setting the parameters of the Hopf model. The feet gait controlled by the CPG controller is shown in Fig. 8. In Fig. 8, the threshold is a value for controlling the duty cycle of the CPG controller.

The time scales of the upward and downward movements of the robot feet can be regulated by changing the threshold. The foot is under the water when the output curve is greater than the threshold, and it is on the water when the output curve is smaller than the threshold. If the robot is disturbed when running on water, its balance keeping ability will be decreased. We can increase the balance keeping ability of the robot by reducing the frequency of water surface slapping through regulating the output threshold.

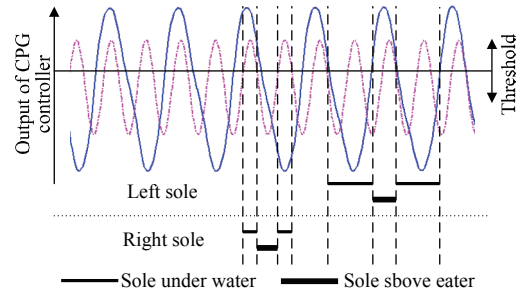


**Fig. 8** Feet gait controlled by the CPG controller.

**4.2 Fuzzy rules of the biped robot**

Gait transition and balance control are two main control objectives. Denote  $\delta$  (see Fig. 9) as the tilt angle between the robot body symmetry plane and the vertical plane,  $d|\delta|/dt$  as the input linguistic variables, and the torque  $\tau$  generated by the balance apparatus as the output linguistic variables. The Mamdani inference algorithm of the parallel fuzzy inference algorithms and the centroid method of the defuzzification methods are adopted to build the fuzzy controller of the robot. The conversion of the input linguistic variables of the fuzzy controller from the basic universe to the discrete universe of fuzzy sets is shown in Table 2.

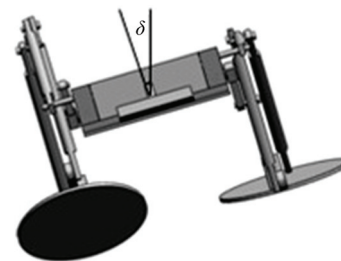


**Fig. 9** Body tilt angle when the robot running on water.



Both  $\delta$  and  $d|\delta|/dt$  have the following seven linguistic variables: NB, NM, NS, Z, PS, PM and PB, so the robot fuzzy controller has 49 rules, which are listed in Table 3. It can be known from Table 3 if  $\delta = \text{NB}$  and  $d|\delta|/dt = \text{NB}$ , then  $\tau = \text{NB}$ , and the other fuzzy inference rules can be deduced in a similar manner.

**Table 2** Conversion of the input linguistic variables

Ranges of $\delta$ (degree)	Values	Ranges of $d \delta /dt$ (degree·s <sup>-1</sup> )	Values
$\delta \geq 30$	-6	$d \delta /dt \leq -60$	-6
$\delta = 25$	-5	$d \delta /dt = -50$	-5
$\delta = 20$	-4	$d \delta /dt = -40$	-4
$\delta = 15$	-3	$d \delta /dt = -30$	-3
$\delta = 10$	-2	$d \delta /dt = -20$	-2
$\delta = 5$	-1	$d \delta /dt = -10$	-1
$\delta = 0$	0	$d \delta /dt = 0$	0
$\delta = -5$	1	$d \delta /dt = 10$	1
$\delta = -10$	2	$d \delta /dt = 20$	2
$\delta = -15$	3	$d \delta /dt = 30$	3
$\delta = -20$	4	$d \delta /dt = 40$	4
$\delta = -25$	5	$d \delta /dt = 50$	5
$\delta \leq -30$	6	$d \delta /dt \geq 60$	6

**Table 3** Fuzzy control rules of the biped robot running on water

$\tau \setminus \delta$	NB	NM	NS	Z	PS	PM	PB
NB	NB	NB	NB	NM	NM	NS	Z
NM	NB	NB	NM	NM	NS	Z	PS
NS	NB	NM	NM	NS	Z	PS	PM
Z	NM	NM	NS	Z	PS	PM	PM
PS	NM	NS	Z	PS	PM	PM	PB
PM	NS	Z	PS	PM	PM	PB	PB
PB	Z	PS	PM	PM	PB	PB	PB

**4.3 CPG-based fuzzy controller design**

The robot body should keep balance when running on water, so we have to keep the tilt angle around zero, which can be achieved by incorporating the CPG controller with the fuzzy control method. In Fig. 10, the control inputs are the tilt angle  $\delta$  and the time differential of its absolute value  $d|\delta|/dt$ . The simulation result of the robot CPG-based fuzzy control system can be got as

Fig. 11, where the horizontal axis represents time  $t$  and the vertical axis represents  $\delta$ , and the maximum value of  $\delta$  is about  $22^\circ$ . When  $t \in [0, 0.75)$ , the body tilt angle increases constantly. When  $t \in [0.75, 1.25)$ , the body tilt angle is converging. After 1.25 s, the system oscillates around 0. The simulation results prove that the robot can keep balance when running on water.

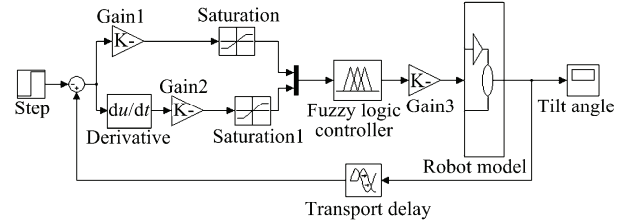


**Fig. 10** CPG-fuzzy control system of the water running biped robot.

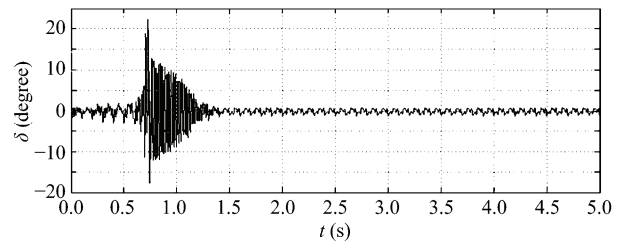


**Fig. 11** Simulation result of the CPG-fuzzy control system.

**5 Experiments**

The prototype of the biped water running robot is shown in Fig. 12. As shown in Fig. 6, the driving system is composed of a motor and a reducer, which are fixed on the main frame. The transmission structure includes a bevel gear pair and a transmission shaft. The bevel gear pair turns the linear motion to the rotational motion around the shaft, and the driving torque is passed to the two propulsion components. A balance apparatus is fitted on the back of the frame, which can keep the robot balance when running on water. When the right foot slaps water surface, the tail fin rotates to left to balance the torque around the body, and rotates to the right

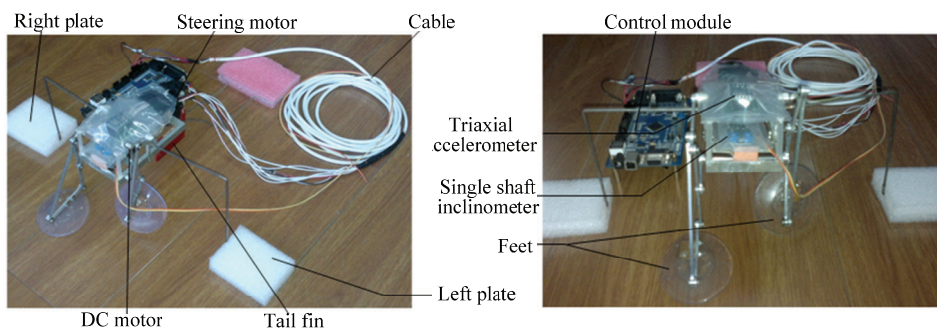


**Fig. 12** Prototype of the biped water running robot.

when the left foot slaps water surface.

Two foamed plastic plates are used to provide the robot buoyancy as shown in Fig. 12. The volumes of the left and right plates are 91.605 cm<sup>3</sup> and 97.712 cm<sup>3</sup> respectively, and the total buoyancy is 1.856 N when they are fully under water. The whole gravity of the robot is 3.2 N, which is larger than the total buoyancy, so the robot will sink when it is placed on the water surface statically. The sequence diagrams of the robot sinking are shown in Fig. 13.

A series of images of the robot running on water are shown in Fig. 14. The robot can walk on water due to the lifting and propulsion force produced by the feet slapping during 1 s to 4 s. We cut off the power supply after 4 s, and the robot stopped slapping and began to sink in water. At last the robot sank totally when the time is 6 s.

The lifting and propulsion force is the decisive factor of the robot's load capacity, that is, the larger the force, the higher the load capacity. We build an experimental platform to test the lifting and propulsion force of the robot. We mount the strain gages on each foot, and the voltage variation of the strain gage is shown

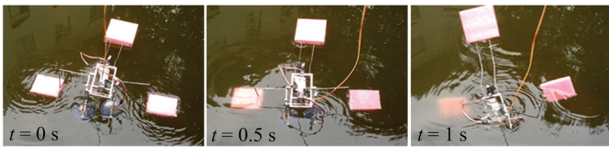


Fig. 13 Sequence diagrams of the robot sinking.

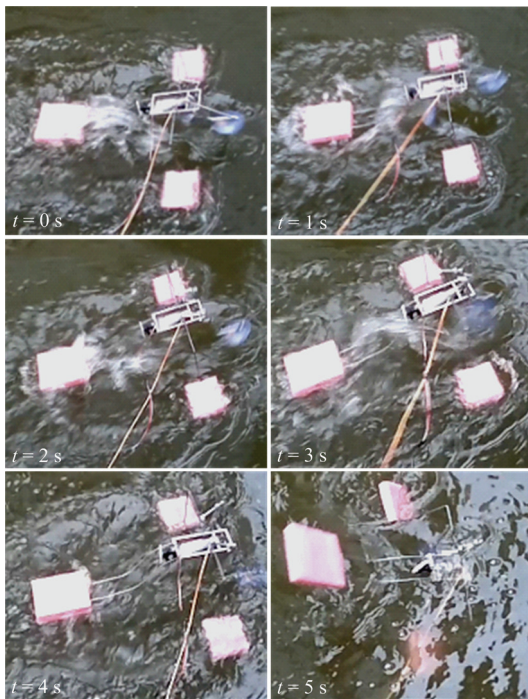


Fig. 14 Sequence diagrams of the robot running on water.

by an oscillograph, from which the lifting and propulsion force can be got. The curve of the lifting and propulsion force is shown in Fig. 15.

The actual force curve in Fig. 15 is similar to that in the simulation as shown in Fig. 3. The peak value of the actual lifting and propulsion force is 2.6 N, which is less than the force value of 4 N in simulation; the valley value of the actual force is about 0.8 N, which is also less than the value of 1.3 N in Fig. 3. The simulation force values are larger than the realistic ones because the transmission efficiency, the pressure of the atmosphere and the deformation of the feet are not considered in simulation.

When the steering engine does not work, the real-time tilt angle curve is shown in Fig. 16. It can be known that the tilt angle is big, and the maximum value is about 13° at the speed of 0.6 m·s<sup>-1</sup>. When the steering engine works with the CPG-fuzzy control system, the real-time tilt angle curve shown that the tilt angle is smaller, whose maximum value is about 5° at the speed of 0.6 m·s<sup>-1</sup>, as shown in Fig. 17.

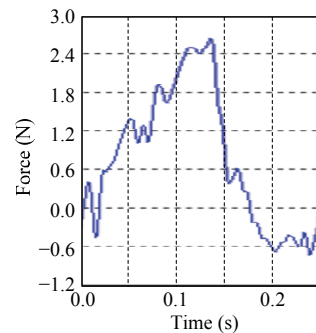


Fig. 15 Force curve measured by the strain gauge.

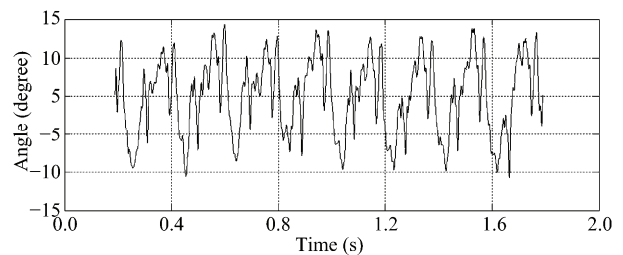


Fig. 16 Real-time tilt angle curve without the steering engine working.

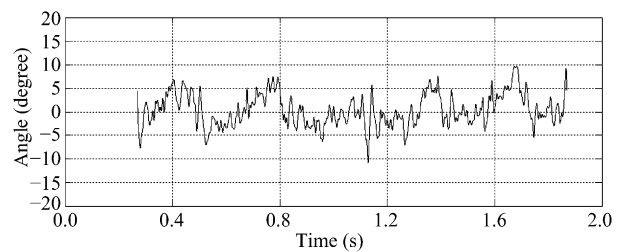


Fig. 17 Real-time tilt angle curve with the steering engine working.

The speed of the robot can be adjusted by controlling the motor speed, and the maximum speed is  $0.9 \text{ m}\cdot\text{s}^{-1}$  before the robot losing balance.

## 6 Conclusion

Inspired by basilisk lizards, a novel biped water running robot was designed in this paper, which offers theoretical and design foundations for developing bionic amphibious biped robot. The virtual prototype of the robot was built by designing the propulsion mechanism with Watt-I planar linkage. Then the CPG-based fuzzy control method was developed to keep the biped robot balance during running on water. The prototype of the robot was made and the water-running experiments were performed. The mean value of the lifting and propulsion force generated by the propulsion mechanism is about 1.3 N, and the maximum speed of the robot running on water is about  $0.9 \text{ m}\cdot\text{s}^{-1}$ .

There still remains lot of work to be done in the future. The algorithms for the robot in straight walking, turning and obstacle avoidance should be further developed, the composite propulsion mechanism of the amphibious biped robot should be designed, and the propulsion movement on both land and water should be implemented by using mode switching control methods.

## Acknowledgement

This work is supported by the National Natural Science Foundation of China (No. 50905175), and the National Program on Key Basic Research Project of China (No. 2011CB302106).

## References

- [1] Gao F. Reflection on the current status and development strategy of mechanism research. *Chinese Journal of Mechanical Engineering*, 2005, **41**, 3–17. (in Chinese)
- [2] Dong X, Wang X. Development of rescue robot technology and its application in disaster. *Journal of Disaster Prevention and Mitigation Engineering*, 2007, **27**, 112–117. (in Chinese).
- [3] Boxerbaum A S, Werk P, Quinn R D, Vaidyanathan R. Design of an autonomous amphibious robot for surf zone operation: Part I – Mechanical design for multi-mode mobility. *Proceedings of the 2005 International Conference on Advanced Intelligent Mechatronics*, Monterey, CA, USA, 2005, 1459–1465.
- [4] Harkins R, Ward J, Vaidyanathan R, Boxerbaum A S, Quinn R D. Design of an autonomous amphibious robot for surf zone operation: Part II – Hardware, control implementation and simulation. *Proceedings of the 2005 IEEE/ASME International Conference on Advanced Intelligent Mechatronics*, Monterey, CA, USA, 2005, 1465–1470.
- [5] Hobson B W, Kemp M, Moody R, Pell C, Vosburgh F. *Amphibious Robot Devices and Related Methods*, USA Patent, 2005, US6974356-B2.
- [6] Song Y S, Sitti M. Surface-tension-driven biologically inspired water strider robots: Theory and experiments. *IEEE Transactions on Robotics*, 2007, **23**, 578–589.
- [7] Floyd S, Sitti M. Design and development of the lifting and propulsion mechanism for a biologically inspired water runner robot. *IEEE Transactions on Robotics*, 2008, **24**, 698–709.
- [8] Floyd S, Keegan T, Palmisano J, Sitti M. A novel water running robot inspired by basilisk lizards. *Proceedings of the IEEE/RSJ Intelligent Robotic Systems Conference*, Beijing, China, 5430–5436.
- [9] Hsieh T, Lauder G. Running on water: Three-dimensional force generation by basilisk lizards. *PNAS*, 2004, **101**, 16784–16788.
- [10] Mirth J A, Chase T R. Circuits and branches of single-degree-of freedom planar linkages. *ASME Journal of Mechanical Design*, 1993, **115**, 223–230.
- [11] Zhen W, Wu K. *Mechanisms and Machine Theory*, 5th ed, Higher Education Press, Beijing, China, 1997. (in Chinese)
- [12] Xu L, Li B, Xu F, Zhao J, Feng B. Optimization synthesis on water running mechanism of biped robot. *Advanced Materials Research*, 2011, **211–212**, 454–459.
- [13] Sugihara T, Nakamura Y, Inoue H. Realtime humanoid motion generation through ZMP manipulation based on inverted pendulum control. *Proceedings of the 2002 IEEE International Conference on Robotics and Automation*, Washington DC, USA, 2002, 1404–1409.
- [14] Or J. A hybrid CPG-ZMP control system for stable walking of a simulated flexible spine humanoid robot. *Neural Networks*, 2010, **23**, 452–460.
- [15] Huang B. *Study on Walking Gait and CPG Control of a Quadruped Robot*, PhD Thesis, Harbin University of Technology, Harbin, China, 2007. (in Chinese)